

A Novel Muscle Synergy Extraction Method to Explain the Equilibrium–point Trajectory and Endpoint Stiffness during Human Upper–limb Movements on a Horizontal Plane

Kanna Uno¹, Takanori Oku¹, Pipatthana Phatiwuttipat¹, Keitaro Koba¹, Yuto Yamashita¹, Kenta Murakami¹,
Mitsunori Uemura¹, Hiroaki Hirai¹, and Fumio Miyazaki¹

Abstract—Based on the idea of synergy to explore the building blocks of movements, this study focused on the muscle space for reaching movements by human upper limbs on a horizontal plane to estimate the relationship among muscle synergies, equilibrium–point (EP) trajectories, and endpoint stiffness in two ways: (1) a novel estimation method that analyzes electromyographic signals under the concept of agonist–antagonist (A–A) muscle pairs and (2) a conventional estimation method that uses mechanical perturbations. The experimental results suggest that (1) muscle activities of reaching movements by human upper limbs are represented by only three functional muscle synergies; (2) each muscle synergy balances the coactivations of A–A muscle pairs; (3) two of the muscle synergies are invariant bases that form an EP trajectory described in polar coordinates centered on a shoulder joint, where one is a composite unit for radial movement and the other is for angular movement; and (4) the third muscle synergy is the invariant basis for additional adjustment of the endpoint stiffness and has some influence on the direction and size of the endpoint stiffness ellipse.

I. INTRODUCTION

Over the past half–century, the idea of synergy has attracted great interest from neuroscientists exploring the building blocks of movements, which may consist of functional modules or composite units of motor primitives [1]. Despite evidence showing that synergy may be an effective solution to the motor redundancy problems inherent to the musculoskeletal system [2], the connection between synergy and the dynamic features of movements has received less attention. Electromyography (EMG) is one of the most effective tools to give insight into how the central nervous system (CNS) solves such problems [3], [4]. EMG signals include fruitful information such as kinematics and stiffness motor commands; separating them is key to solving the physiological mechanism for human motor control.

There are two popular hypotheses to explain motor control: Bernstein’s muscle synergy hypothesis [2] and Feld-

man’s EP hypothesis (λ model) [5]. Bernstein suggested that the CNS avoids the complexity of the redundant musculoskeletal structure and reduces the number of control variables by coupling small groups of muscles into more global synergic units. In contrast, Feldman suggested that the CNS sends motor commands, including reciprocal and coactivation commands, to peripheral muscles; the reciprocal and coactivation commands help control the equilibrium–point (EP) and stiffness, respectively. Several engineering studies have deepened these pioneering ideas. Artemiadis et al. reduced nine EMG signals related to the motion of a human upper limb to two–dimensional manifolds by a statistical method, and defined them as muscle synergies; they used the synergies to estimate the hand position and control of a robot arm [6]. Santello et al. applied principal component analysis to the data for the finger joint angles and revealed that almost all of the hand postures can be represented by only the first and second principal components; they considered a few postural synergies to regulate the general shape of the hand [7]. Gomi et al. measured the endpoint stiffness during multi–joint movement of a human upper limb with the mechanical perturbations and estimated the EP trajectory with a dynamic model of the limb; they revealed that the size and direction of the endpoint stiffness is regulated at all times even for a simple reaching movement, emphasizing the complexity involved in EP trajectory [8]. In these studies, the motor functions of the synergies or the relationship between muscle synergy, EP trajectory, and endpoint stiffness have not been clarified. Thus, we focused on the cooperative effect of agonist–antagonist (A–A) muscle pairs around a joint, which may be related to the EP or stiffness and may be a component of muscle synergy [9]–[12]. Our previous studies revealed that the ratio of the A–A muscle activity level (A–A ratio) representing a reciprocal command helps control the joint EP angle and that the sum of the A–A muscle activity level (A–A sum) representing a coactivation command helps regulate the joint stiffness; they are suitable for understanding the cooperation of muscles, EP, and stiffness. We applied a statistic method under the A–A concept to EMG signals during multi–joint movement in the static [9] and dynamic [10] conditions, and extracted muscle synergies successfully. As a next step, in this study we clarified the relationship between the muscle synergy, EP trajectory, and endpoint stiffness in terms of physical motor functions expressed by muscle synergies. We propose a novel

This work was performed at Osaka University. ¹All of authors are with the Department of Mechanical Science and Bioengineering, Graduate School of Engineering Science, Osaka University. The authors’ e-mail addresses are uno@robotics.me.es.osaka-u.ac.jp
oku@robotics.me.es.osaka-u.ac.jp
phatiwuttipat@robotics.me.es.osaka-u.ac.jp
koba@robotics.me.es.osaka-u.ac.jp
yamashita@robotics.me.es.osaka-u.ac.jp
murakami@robotics.me.es.osaka-u.ac.jp
uemura-m@me.es.osaka-u.ac.jp
hirai@me.es.osaka-u.ac.jp
miyazaki@me.es.osaka-u.ac.jp

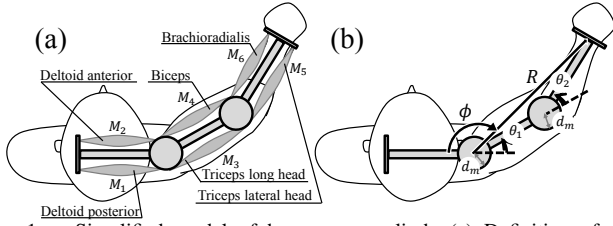


Fig. 1. Simplified model of human upper limb. (a) Definition of six muscles; (b) Definition of hand position and joint angles.

extraction method of muscle synergies from musculoskeletal modeling; the method can be explained by using the analogy between the human musculoskeletal system and A–A pneumatic artificial muscle system. Unlike Shin’s [3] method, our proposed method requires neither detailed modeling nor high calculation costs. In order to test the validity, we extracted muscle synergies from actual EMG signals of an upper limb during two kinds of reaching movement (longitudinal and lateral direction), which we compared for different tasks and subjects. Finally, we estimated the EP trajectory and endpoint stiffness with our proposed method and with the conventional perturbation method respectively; the physical roles of the three muscle synergies were investigated.

II. NOVEL MUSCLE SYNERGY EXTRACTION METHOD

Consider a two-link structure with three pairs of muscles as a simplified human upper limb (**Fig. 1**): mono-articular muscle pairs around the shoulder and elbow and a bi-articular muscle pair between the shoulder and elbow joints. This system is redundant: two degrees of freedom (DOFs) for the endpoint and six for the muscles. Pneumatic artificial muscles (PAMs) and human muscles are similar in terms of having complex spring characteristics where the stiffness increase and length decrease with the muscle activity level. Therefore, this paper assumed that the simplified PAMs can be considered to be equivalent to human muscles [11]. When these six PAMs are under equilibrium conditions, P_i is the internal pressure of PAM M_i , $F(P_i)$ is the contractile force, $K(P_i)$ is the muscle stiffness, $l(P_i)$ is the muscle length, and $l_0(P_i)$, ($i = 1, 2, \dots, 6$) is the natural muscle length; the following conditions are satisfied provided that moment arms d_m and muscle initial lengths l of the PAMs are equal. For humans, the lengths of the upper arm and forearm are almost the same, so their individual link lengths can be simplified to L .

$$F(P_1) - F(P_2) + F(P_3) - F(P_4) = 0 \quad (1)$$

$$F(P_3) - F(P_4) + F(P_5) - F(P_6) = 0 \quad (2)$$

Equations 1 and 2 satisfy the equilibrium state condition of the system. According to Ariga et al. [11], C_1, C_2, C_3, C_4 are constant coefficients that represent the properties of PAMs and that satisfy the following conditions:

$$l_0(P_i) = C_1/K(P_i) + C_2 \quad (3)$$

$$F(P_i) = K(P_i)(l(P_i) - l_0(P_i)) \quad (4)$$

In addition, the muscle stiffness $K(P_i)$ and internal pressure P_i are as follows:

$$K(P_i) = C_3(P_i - C_4) \quad (5)$$

TABLE I

DEFINITIONS AND FUNCTIONS OF A–A RATIO AND A–A SUM (M_i MEANS \hat{P}_i FOR PAM SYSTEM AND m_i FOR BIOLOGICAL SYSTEM).

label	definition	function
r_1	$\frac{M_1}{M_1+M_2}$	shoulder-joint angle extension
r_2	$\frac{M_3}{M_3+M_4}$	shoulder & elbow-joint angle extension
r_3	$\frac{M_5}{M_5+M_6}$	elbow-joint angle extension
s_1	$M_1 + M_2$	shoulder-joint stiffness increase
s_2	$M_3 + M_4$	shoulder & elbow-joint stiffness increase
s_3	$M_5 + M_6$	elbow-joint stiffness increase

Using $\hat{P}_i = P_i - C_4$, the following equation is satisfied:

$$K(\hat{P}_i) = C_3\hat{P}_i \quad (6)$$

According to the geometric conditions,

$$d_m\theta_1 = l(P_1) - l = l - l(P_2) \quad (7)$$

$$d_m(\theta_1 + \theta_2) = l(P_3) - l = l - l(P_4) \quad (8)$$

$$d_m\theta_2 = l(P_5) - l = l - l(P_6) \quad (9)$$

The above are substituted into eqs. (1) and (2). If C_1, C_2, C_3, C_4 are equal for all six muscles, the following condition is satisfied:

$$\begin{pmatrix} K(P_1)+K(P_2) & K(P_3)+K(P_4) \\ +K(P_3)+K(P_4) & K(P_3)+K(P_4) \\ K(P_3)+K(P_4) & +K(P_5)+K(P_6) \end{pmatrix} \begin{pmatrix} d_m\theta_1 \\ d_m\theta_2 \end{pmatrix} = (C_2 - l) \begin{pmatrix} K(P_1) - K(P_2) + K(P_3) - K(P_4) \\ K(P_3) - K(P_4) + K(P_5) - K(P_6) \end{pmatrix} \quad (10)$$

$$\Rightarrow \begin{pmatrix} \hat{P}_1 + \hat{P}_2 + \hat{P}_3 + \hat{P}_4 & \hat{P}_3 + \hat{P}_4 \\ \hat{P}_3 + \hat{P}_4 & \hat{P}_3 + \hat{P}_4 + \hat{P}_5 + \hat{P}_6 \end{pmatrix} \begin{pmatrix} \theta_1 \\ \theta_2 \end{pmatrix} = \frac{C_2 - l}{d_m} \begin{pmatrix} \hat{P}_1 - \hat{P}_2 + \hat{P}_3 - \hat{P}_4 \\ \hat{P}_3 - \hat{P}_4 + \hat{P}_5 - \hat{P}_6 \end{pmatrix} \quad (11)$$

Here, the A–A ratios r_i and A–A sums s_i , ($i = 1, 2, 3$) are defined for the internal pressure \hat{P}_i [11]:

$$r_i = \hat{P}_{2i-1} / (\hat{P}_{2i-1} + \hat{P}_{2i}) \quad (12)$$

$$s_i = \hat{P}_{2i-1} + \hat{P}_{2i} \quad (13)$$

Table I physically defines each A–A ratio and A–A sum. By the deformation of eq. (11) with r_i and s_i , the following equation is satisfied:

$$\begin{pmatrix} \theta_1 \\ \theta_2 \end{pmatrix} = \frac{2(C_2 - l)}{d_m} \begin{pmatrix} s_1 + s_2 & s_2 \\ s_2 & s_2 + s_3 \end{pmatrix}^{-1} \begin{pmatrix} s_1 & s_2 & 0 \\ 0 & s_2 & s_3 \end{pmatrix} \begin{pmatrix} r_1 - 1/2 \\ r_2 - 1/2 \\ r_3 - 1/2 \end{pmatrix} = \frac{2(C_2 - l)}{d_m} \begin{pmatrix} \mathbf{q}_1^T \\ \mathbf{q}_2^T \end{pmatrix} \begin{pmatrix} r_1 - 1/2 \\ r_2 - 1/2 \\ r_3 - 1/2 \end{pmatrix} \quad (14)$$

where

$$\mathbf{q}_1 = \frac{1}{s_1s_2 + s_2s_3 + s_3s_1} (s_1s_2 + s_3s_1, s_2s_3, -s_2s_3)^T \quad (15)$$

$$\mathbf{q}_2 = \frac{1}{s_1s_2 + s_2s_3 + s_3s_1} (-s_1s_2, s_1s_2, s_3s_1 + s_2s_3)^T \quad (16)$$

By using eq. (14), the endpoint EP velocity $(\dot{R}, \dot{\phi})^T$ shown in polar coordinates (**Fig. 1(b)**) can be expressed by using A–A ratios r_i and A–A sums s_i . The endpoint EP in polar coordinates $\mathbf{p} = (R, \phi)^T$ can be expressed by the joint angles $(\theta_1, \theta_2)^T$:

$$\begin{pmatrix} R \\ \phi \end{pmatrix} = \begin{pmatrix} 2L\cos\frac{\theta_2}{2} \\ \pi - \theta_1 - \frac{\theta_2}{2} \end{pmatrix} \quad (17)$$

If both sides of eqs. (14) and (17) are differentiated with respect to time, and \mathbf{q}_1 and \mathbf{q}_2 are assumed to be constant

around the EP:

$$\dot{\mathbf{p}} = \begin{pmatrix} 0 & -L\sin\frac{\theta_2}{2} \\ -1 & -\frac{1}{2} \end{pmatrix} \begin{pmatrix} \dot{\theta}_1 \\ \dot{\theta}_2 \end{pmatrix} = \begin{pmatrix} C_5(\theta_2) & 0 \\ 0 & C_6 \end{pmatrix} \begin{pmatrix} \mathbf{q}_2^T \\ (\mathbf{q}_1 + \frac{1}{2}\mathbf{q}_2)^T \end{pmatrix} \begin{pmatrix} \dot{r}_1 \\ \dot{r}_2 \\ \dot{r}_3 \end{pmatrix} \quad (18)$$

where $C_5(\theta_2) = \frac{2L(l-C_2)}{d_m}\sin\frac{\theta_2}{2}$ and $C_6 = \frac{2(l-C_2)}{d_m}$ are values dependent on the muscle length, link length, moment arm, and elbow angle θ_2 . $C_5(\theta_2)$ can be approximated as a constant C_5 in most cases. Eq. (18) shows that the two vectors \mathbf{q}_2 and $(\mathbf{q}_1 + \frac{1}{2}\mathbf{q}_2)$, which are dependent on A–A sums, compose a partial space, and the projection of A–A ratio velocity vector $\dot{\mathbf{r}} = (\dot{r}_1, \dot{r}_2, \dot{r}_3)^T$ to the partial space allows the EP velocity to be estimated. The base radial, angular, and orthogonal vectors to both the radial and angular directions are as follows:

$$\mathbf{u}_R = \mathbf{q}_2/|\mathbf{q}_2| \quad (19)$$

$$\mathbf{u}_\phi = (\mathbf{q}_1 + \frac{\mathbf{q}_2}{2})/|\mathbf{q}_1 + \frac{\mathbf{q}_2}{2}| \quad (20)$$

$$\mathbf{u}_{R \times \phi} = (\mathbf{u}_R \times \mathbf{u}_\phi)/|\mathbf{u}_R \times \mathbf{u}_\phi| \quad (21)$$

These base vectors indicate the distribution of A–A ratio vectors for each direction. \mathbf{u}_R , \mathbf{u}_ϕ are defined as the radial directional muscle synergy vector and angular directional muscle synergy vector, respectively. $\mathbf{u}_{R \times \phi}$ is defined as the null directional muscle synergy vector. The A–A ratios $\bar{\mathbf{r}}$ are averaged to define variations of the A–A ratios $d\mathbf{r} = \mathbf{r} - \bar{\mathbf{r}}$. The inner products $w_R = \mathbf{u}_R \cdot d\mathbf{r}$, $w_\phi = \mathbf{u}_\phi \cdot d\mathbf{r}$, and $w_{R \times \phi} = \mathbf{u}_{R \times \phi} \cdot d\mathbf{r}$ are defined as muscle synergy scores. By integrating eq. (18), the following conditions are satisfied:

$$R \propto \mathbf{u}_R \cdot d\mathbf{r} \quad (22)$$

$$\phi \propto \mathbf{u}_\phi \cdot d\mathbf{r} \quad (23)$$

III. EXPERIMENT

A. Method

The subject moved his hand from one position to the other, and a mechanical perturbation was randomly applied to the hand. The joint stiffness can be calculated according to the magnitude of the displacement of the hand. Subjects A, B, and C were healthy teenage males who volunteered to take part in this experiment. The upper limb of a subject was suspended from the ceiling to compensate for gravity, and limb movement on a horizontal plane was restricted. Both shoulders were fixed to a chair with harnesses. In order to conceptualize the upper limb as a two-link construction, the wrist joint was fixed with a plastic cuff. A laser pointer and the manipulandum tip (PHANTOM Premium 3.0/6DOF, SensAble Technologies Inc., sampling rate 100 [Hz]) were fixed to the palm pointing vertically downward. A paper showing the start and end positions and the movement direction was fixed on the work space to confirm the hand position by the irradiation of the laser pointer. **Figures 1** and **2(b)** show the position and definition of the joints in polar and Cartesian coordinates and the three pairs of muscles contributing to human upper limb motion on a horizontal plane. The four markers on the left shoulder, right shoulder, right elbow, and right hand were tracked by a motion capture system (OptiTrack, NaturalPoint, Inc.) to measure the shoulder angle θ_1 and elbow angle θ_2 . The sampling rate was 100

[Hz]. EMG recording were synchronized with motion capture system and performed with a biological amplifier (WEB-5000, Nihon Koden Corp.) and AD converter (PowerLab, AD Instruments Inc.) at a sampling rate of 1000 [Hz]. The lateral reaching movement started at position 1 and ended at position 2. Each subject kept the endpoint at position 1 for 1 [s], moved it to position 2 in 1 [s], and kept it there for 1 [s] as one task. A metronome was used to cue the movements. The interval time between tasks was anywhere between 2 and 2.5 [s]. The perturbations were timed to occur at five positions: just before the start of the movement, at a quarter, half, and three-quarters of the path, and just before the end of the movement. One of these positions was selected at random. The perturbation periods were sufficiently short (0.2 [s]). The perturbations occurred in one of eight directions spaced 45 [deg] apart, which was selected at random. One experimental set comprised 40 tasks, and eight sets were measured. **Figure 2(c)** shows the timings and directions of the perturbations. The amplitude of the perturbation force was set to 6 or 8 [N] depending on the physique of the subject. Additionally the longitudinal reaching movements from position 3 to position 4 were measured 40 times without perturbations.

B. Processing

1) *EMG signals*: The noise of the EMG signals was filtered out with bandpass filter (10–450 [Hz]); the signals were then rectified, smoothed with a 5 [Hz] lowpass filter, down-sampled to 100 [Hz], and then normalized with the maximum voluntary contraction (MVC). m_i , ($i = 1 \dots 6$) represents the EMG signal (%MVC) of each muscle during the task. A–A ratios are defined as $r_i = \frac{m_{2i-1}}{m_{2i-1} + m_{2i}}$, and A–A sums are defined as $s_i = m_{2i-1} + m_{2i}$ (**Table I**).

2) *Joint stiffness and A–A sums*: For an artificial muscle antagonistic drive system, the joint stiffness under the static condition \mathbf{K}_θ can be expressed with the A–A sum \mathbf{s} . The joint torques of the shoulder and elbow τ_1, τ_2 are expressed with the muscle stiffness $K(P_i)$ and joint angles θ_1, θ_2 as

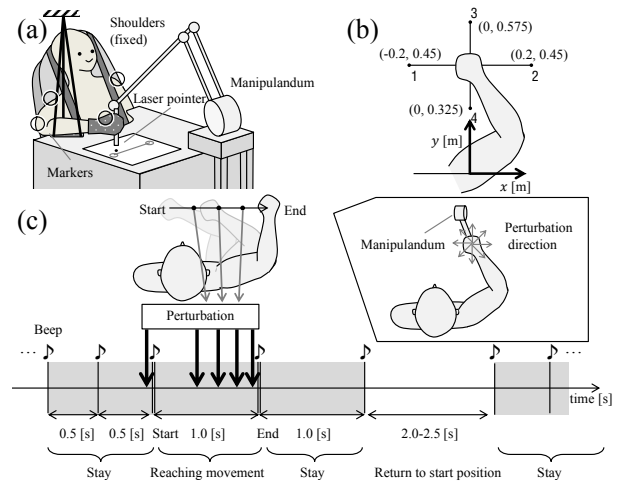


Fig. 2. (a) Experimental setup to measure endpoint stiffness during reaching movement; (b) Start and end positions of reaching movement; (c) Timing of beeps and perturbations.

follows:

$$\begin{pmatrix} \tau_1 \\ \tau_2 \end{pmatrix} = d_m^2 \begin{pmatrix} (K(P_1)+K(P_2))\theta_1 \\ +(K(P_3)+K(P_4))(\theta_1+\theta_2) \\ (K(P_3)+K(P_4))(\theta_1+\theta_2) \\ +(K(P_5)+K(P_6))\theta_2 \end{pmatrix} = C_3 d_m^2 \begin{pmatrix} s_1\theta_1+s_2(\theta_1+\theta_2) \\ s_2(\theta_1+\theta_2)+s_3\theta_3 \end{pmatrix} \quad (24)$$

$$\Rightarrow \mathbf{K}_\theta = \frac{\partial(\tau_1, \tau_2)^T}{\partial(\theta_1, \theta_2)} = C_3 d_m^2 \begin{pmatrix} s_1+s_2 & s_2 \\ s_2 & s_2+s_3 \end{pmatrix} \quad (25)$$

Here C_3 and d_m are constant and the joint stiffness \mathbf{K}_θ can be expressed by linear transformation of the A–A sums.

3) *Endpoint stiffness estimated from EMG signals:* Assuming that eq. (25) is also valid for a human as described in the previous section, a constant value k_s [Nm/rad] can be used to transform the A–A sum s to the joint stiffness \mathbf{K}_s .

$$\mathbf{K}_s = k_s \begin{pmatrix} s_1+s_2 & s_2 \\ s_2 & s_2+s_3 \end{pmatrix} \quad (26)$$

Here, k_s was determined to be 200 [Nm/rad] for subject A, 250 [Nm/rad] for B, and 100 [Nm/rad] for C according to the subject–dependent EMG levels. In order to verify the hypothesis that the null directional muscle synergy helps regulate the size and direction of the endpoint stiffness under the dynamic condition, we added the absolute value of the null directional muscle synergy score $|w_{R \times \phi}|$ to each component of \mathbf{K}_s . The renewed joint stiffness \mathbf{K}_{s+n} is expressed by the constant k_n as follows:

$$\mathbf{K}_{s+n} = \mathbf{K}_s + k_n \begin{pmatrix} |w_{R \times \phi}| & |w_{R \times \phi}| \\ |w_{R \times \phi}| & |w_{R \times \phi}| \end{pmatrix} \quad (27)$$

The joint stiffness estimated from the EMG signals \mathbf{K}_{s+n} was transformed by the Jacobian $\mathbf{J} = \frac{\partial(x, y)^T}{\partial(\theta_1, \theta_2)}$ to the endpoint stiffness $\mathbf{K}_x^{\text{emg}_{s+n}}$.

$$\mathbf{K}_x^{\text{emg}_{s+n}} = (\mathbf{J}^T)^{-1} (\mathbf{K}_{s+n}) \mathbf{J}^{-1} \quad (28)$$

Here, k_n was determined to be 150 [Nm/rad] for subject A, 200 [Nm/rad] for B, and 50 [Nm/rad] for C. This was done by trial and error. In order to compare the role of the null directional muscle synergy, the endpoint stiffness $\mathbf{K}_x^{\text{emg}_s}$ was also estimated from only the A–A sums as follows:

$$\mathbf{K}_x^{\text{emg}_s} = (\mathbf{J}^T)^{-1} (\mathbf{K}_s) \mathbf{J}^{-1} \quad (29)$$

4) *EP trajectory estimated from EMG signals:* The endpoint EP was estimated from muscle synergy scores. The extraction method is given in the previous section. The muscle synergy scores $w_R (= \mathbf{u}_R \cdot d\mathbf{r})$ and $w_\phi (= \mathbf{u}_\phi \cdot d\mathbf{r})$ were normalized; the polar coordinates of the endpoint during the resting states before and after the reaching movement $(R_{\text{start}}, \phi_{\text{start}})^T, (R_{\text{end}}, \phi_{\text{end}})^T$ were used to linearly transform the muscle synergy scores $(w_{R, \text{start}}, w_{\phi, \text{start}})^T, (w_{R, \text{end}}, w_{\phi, \text{end}})^T$ to the estimated endpoint position in polar coordinates $\mathbf{p}_{\text{est}} = (R_{\text{est}}, \phi_{\text{est}})^T$.

$$R_{\text{est}} = \frac{R_{\text{end}} - R_{\text{start}}}{w_{R, \text{end}} - w_{R, \text{start}}} (w_R - w_{R, \text{start}}) + R_{\text{start}} \quad (30)$$

$$\phi_{\text{est}} = \frac{\phi_{\text{end}} - \phi_{\text{start}}}{w_{\phi, \text{end}} - w_{\phi, \text{start}}} (w_\phi - w_{\phi, \text{start}}) + \phi_{\text{start}} \quad (31)$$

\mathbf{p}_{est} was transformed to Cartesian coordinates and $\mathbf{x}_{\text{est}} = (x_{\text{est}}, y_{\text{est}})^T = (R_{\text{est}} \cos(\pi - \phi_{\text{est}}), R_{\text{est}} \sin(\pi - \phi_{\text{est}}))^T$ was defined as the endpoint EP estimated from muscle synergy scores.

5) *Endpoint stiffness estimated from perturbation method:* The endpoint movement was yielded by both the displace-

ment from robotic perturbations and the voluntary reaching movement, when we use the perturbation method to estimate the endpoint stiffness. In order to remove the effect of perturbations on the reaching movement, the average joint angles during the reaching movement without perturbation $\Theta(t) = (\theta_1(t), \theta_2(t))^T$ were assumed to determine the average trajectory of the reaching movement. The displacement by perturbation $\delta\Theta(t) = (\delta\theta_1(t), \delta\theta_2(t))^T$ was assumed to be the displacement from the start of the perturbation $\Theta_{s, i}$ minus the average displacement from the start of perturbation Θ_{sav} , where $i = 1, 2, \dots, 8$ means the direction of perturbation, t_s means the perturbation start moment, and T means the calculation term to estimate the stiffness, which was set to 0.4 [s].

$$t_s \leq t \leq t_s + T \quad (32)$$

$$\Theta_{s, i}(t) = \Theta_i(t) - \Theta_i(t_s), (i = 1, 2, \dots, 8) \quad (33)$$

$$\Theta_{\text{sav}}(t) = \frac{1}{n} \sum_{i=1}^n \Theta_{s, i}(t), (n = 8) \quad (34)$$

$$\delta\Theta_i(t) = \Theta_{s, i}(t) - \Theta_{\text{sav}}(t) \quad (35)$$

When a perturbation is given, the manipulandum is controlled to produce a constant force $\delta\mathbf{f}_i(t)$.

$$\delta\mathbf{f}_i(t) = \begin{cases} (0, 0)^T & (t < t_s) \\ f(\cos \frac{\pi i}{4}, \sin \frac{\pi i}{4})^T & (t_s \leq t \leq t_s + T) \\ (0, 0)^T & (t_s + T < t) \end{cases} \quad (36)$$

f was 8 [N] for subject A and 6 [N] for B and C. When transformed to a joint space, this force becomes the perturbation torque $\delta\boldsymbol{\tau}(t) = \mathbf{J}^T \delta\mathbf{f}(t)$. The relationship between $\Theta(t), \delta\Theta(t), \delta\boldsymbol{\tau}(t)$, inertia matrix \mathbf{I} , Coriolis and centrifugal forces \mathbf{H} , joint viscosity matrix $\mathbf{D} = \begin{pmatrix} D_{ss} & D_{se} \\ D_{es} & D_{ee} \end{pmatrix}$, and joint

stiffness matrix $\mathbf{K}_\theta = \begin{pmatrix} K_{ss} & K_{se} \\ K_{es} & K_{ee} \end{pmatrix}$ is as follows:

$$\mathbf{I} = \begin{pmatrix} Z_1 + 2Z_2 \cos\theta_2 & Z_3 + Z_2 \cos\theta_2 \\ Z_3 + Z_2 \cos\theta_2 & Z_3 \end{pmatrix} \quad (37)$$

$$\mathbf{H} = \begin{pmatrix} -Z_2 \sin\theta_2 (\dot{\theta}_2^2 + 2\dot{\theta}_1 \dot{\theta}_2) \\ Z_2 \dot{\theta}_1^2 \sin\theta_2 \end{pmatrix} \quad (38)$$

$$\mathbf{I} \delta\ddot{\Theta} + \frac{\partial \mathbf{H}}{\partial \Theta} \delta\dot{\Theta} + \left(\frac{\partial \mathbf{I}}{\partial \Theta} \ddot{\Theta} + \frac{\partial \mathbf{H}}{\partial \Theta} \dot{\Theta} \right) \delta\Theta = -\mathbf{D} \delta\dot{\Theta} - \mathbf{K}_\theta \delta\Theta + \delta\boldsymbol{\tau}_{\text{ext}} \quad (39)$$

Z_1, Z_2 , and Z_3 are constants dependent on the mass of the link and position of the center of gravity, but independent of the posture of the body. The data under the static condition before the reaching movement leads to the matrix $\Xi(\Theta(t), \dot{\Theta}(t), \ddot{\Theta}(t), \delta\Theta(t), \delta\dot{\Theta}(t), \delta\ddot{\Theta}(t)) \in \mathbb{R}^{2 \times 11}$. This matrix satisfies

$$\Xi \cdot (Z_1 Z_2 Z_3 D_{ss} D_{se} D_{es} D_{ee} K_{ss} K_{se} K_{es} K_{ee})^T = \delta\boldsymbol{\tau}_{\text{ext}}(t) \quad (40)$$

\mathbf{I}, \mathbf{D} , and \mathbf{K}_θ can be calculated using the pseudo inverse matrix Ξ^+ . For the next step, the estimated parameters Z_1, Z_2 , and Z_3 are used to calculate \mathbf{D} and \mathbf{K}_θ once more under the dynamic condition. The dynamic equation (39) and calculation method for the parameters are explained in [8] in detail. In [8], the parameters had averages of $Z_1 = 0.39$ [Nm/(rad/s²)], $Z_2 = 0.14$ [Nm/(rad/s²)], and $Z_3 = 0.13$ [Nm/(rad/s²)], which were about half or one-third the parameter values in this study (Table II). This difference

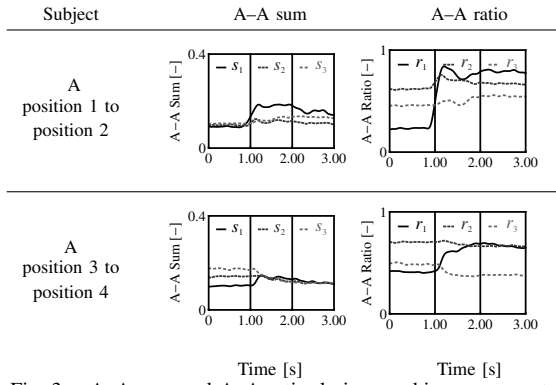


Fig. 3. A–A sum and A–A ratio during reaching movement.

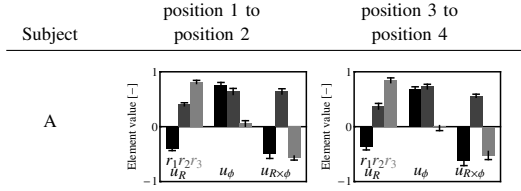


Fig. 4. Synergy vectors during reaching movement.

was due to the support method with the plastic cuff and handle. The endpoint stiffness matrix $\mathbf{K}_x^{\text{ptb}}$ can be expressed by \mathbf{K}_θ , Z_1 , Z_2 , Z_3 , and internal forces \mathbf{F}_{in} as follows:

$$\mathbf{K}_x^{\text{ptb}} = (\mathbf{J}^T)^{-1} (\mathbf{K}_\theta + \frac{\partial \mathbf{J}^T}{\partial \Theta} \mathbf{F}_{\text{in}}) \mathbf{J}^{-1} \quad (41)$$

6) *EP trajectory estimated from perturbation method:* By using the estimated joint stiffness \mathbf{K}_θ and joint viscosity \mathbf{D} , the endpoint EP trajectory \mathbf{x}_{eq} can be computed according to the following formula provided that the joint torque caused by the manipulandum is $\boldsymbol{\tau}_{\text{ext}} = \mathbf{J}^T \mathbf{F}_{\text{ext}}$, $\mathbf{F}_{\text{ext}} = (-15, 0)^T$ [N]:

$$\Theta_{\text{eq}} = \mathbf{K}_\theta^{-1} (\mathbf{I} \ddot{\Theta} + \mathbf{H}(\dot{\Theta}, \Theta) + \mathbf{D} \dot{\Theta} - \boldsymbol{\tau}_{\text{ext}}) + \Theta \quad (42)$$

$$\mathbf{x}_{\text{eq}} = \Phi(\Theta_{\text{eq}}) \quad (43)$$

Here, Φ is a forward kinematics function. Using the link lengths L_1 , L_2 of the upper arm and forearm, the function is described as follows:

$$\Phi(\theta_1, \theta_2) = (L_1 \cos \theta_1 + L_2 \cos(\theta_1 + \theta_2), L_1 \sin \theta_1 + L_2 \sin(\theta_1 + \theta_2))^T \quad (44)$$

\mathbf{I} and \mathbf{H} are computed by Z_1 , Z_2 , Z_3 and Θ . \mathbf{D} and \mathbf{K}_θ were up-sampled to 20 [Hz] with a spline complement over 1 [s] of the reaching movement with the perturbations.

C. Results

Figure 3 shows the transitions of the A–A sums and A–A ratios. **Figure 4** shows the extracted muscle synergy vectors.

Figure 5 shows the endpoint stiffness estimated with the perturbation method, A–A sums, and both the A–A sums and null directional muscle synergy score. **Figure 6** shows the x component of the EP trajectory \mathbf{x}_{eq} estimated from the

TABLE II

ESTIMATED PARAMETERS Z_1 , Z_2 , AND Z_3 .

Subject	Z_1 [Nm/(rad/s ²)]	Z_2 [Nm/(rad/s ²)]	Z_3 [Nm/(rad/s ²)]
A	1.35844	0.32626	0.67764
B	0.95359	0.37478	0.35623
C	0.70989	0.22633	0.34516

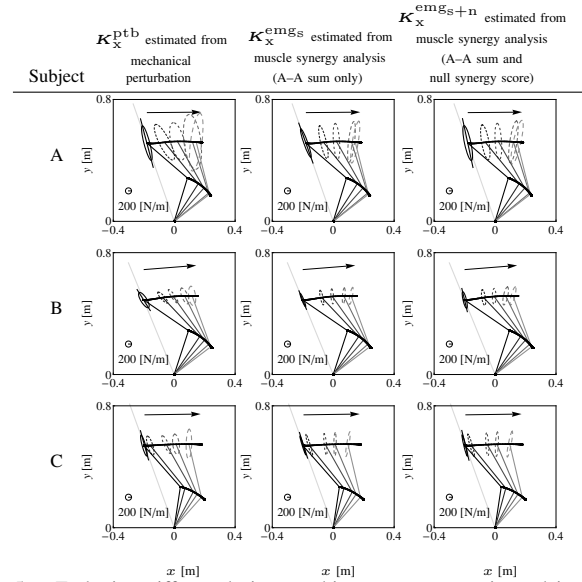


Fig. 5. Endpoint stiffness during reaching movement estimated in three ways; perturbation method, muscle synergy analysis (A–A sum only), and muscle synergy analysis (A–A sum and null synergy score).

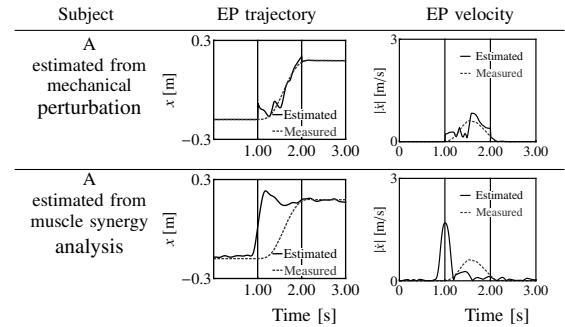


Fig. 6. EP trajectory and EP velocity estimated in two ways; perturbation method and muscle synergy analysis.

perturbation method, the EP velocity $|\dot{\mathbf{x}}_{\text{eq}}|$, the x component of the EP trajectory \mathbf{x}_{est} estimated from the muscle synergy scores w_R , w_ϕ , and the EP velocity $|\dot{\mathbf{x}}_{\text{est}}|$.

D. Discussion

1) *Common muscle synergies:* The subjects showed some differences in the transitions of the A–A ratios and A–A sums; however, both the radial and angular directional muscle synergy vectors of the subjects (A, B, and C) and for movement directions (lateral and longitudinal) were almost the same. All of the inner products of the vectors were more than 0.94, respectively. **Figures 3** and **4** show the results of subject A as a representative example; all the subjects showed similar tendencies. Therefore, the motion base vectors are not different even if different tasks are performed. Based upon the above results, we concluded that the proposed method can extract muscle synergies independent of the task or subject. For the radial muscle synergy vector \mathbf{u}_R in **Fig. 4**, the bi-articular muscle pairs supported elbow joint extension when subjects moved their hand in the positive radial direction. For the angular muscle synergy vector \mathbf{u}_ϕ , the mono-articular muscle pair of the shoulder joint and the bi-articular muscle pair cooperated

to act on the shoulder joint motion, and the EP of the elbow joint was not controlled when subjects moved their hand in the positive angular direction. Compared with the muscle synergies extracted from a statistical technique [9], the muscle synergies discussed here represent clear kinematic functions. On the other hand, the null directional synergy vector $\mathbf{u}_{R \times \phi}$ had almost the same range of r_1, r_3 and an odd sign of r_2 . Therefore, the muscle coordination of the null directional muscle synergy showed antagonism caused by the two mono-articular muscle pairs and bi-articular muscle pair. If the A-A ratios changed to the null direction, the EP of the endpoint had no effect. If the null directional muscle synergy score increased, the EP of the shoulder (or elbow) joint of the mono-articular muscle pair became far from the EP of the joint of the bi-articular muscle pair, and the shoulder (or elbow) joint was stretched to both the extension and flexion sides; this increased the joint stiffness. In conclusion, the null directional muscle synergy can effectively regulate the joint stiffness but not the joint EP.

2) *Endpoint stiffness*: **Figure 5** shows that the endpoint stiffness estimated from the perturbation method increased right after the start and just before the end of the reaching movement. This tendency corresponded with the previous study [8]. In addition, the stiffness ellipse during movement slightly tilted from the direction connecting the right hand and right shoulder. This clarified that the direction of the stiffness is regulated during movement. **Figure 5** also shows that the direction of the stiffness estimated from the A-A sums and null directional muscle synergy score were oriented almost vertically to the trajectory and slightly tilted from the direction connecting the right hand and right shoulder. This is more similar to the tendency from the perturbation method than that from only A-A sums. Therefore, using both may allow the endpoint stiffness to be estimated closer to the measured value.

3) *EP trajectory and velocity*: The tendency of the EP trajectory estimated from the perturbation method in **Fig. 6** corresponded with the previous study [8]. Although the actual endpoint velocity profile was bell-shaped, the EP velocity profile estimated from the perturbation method showed multiple peaks. This multipeak shape was also seen in the estimation from the muscle synergy scores (**Fig. 6**). The multipeak shape of the EP velocity from the muscle synergy scores shows that the EMG signals may be generated from a superposition of several waves (submovements). In particular, a peak just before the start of the movement seems to be a feedforward motor command from the CNS to start moving the hand. In contrast, a peak just before the end of the movement is considered to be a feedback motor command to adjust the hand position. If this multipeak shape of muscle synergy scores represents the multipeak shape of the EP velocity profile, this novel extraction method shows indirect evidence that motor control is generated by a discrete combination of feedforward and feedback motor commands.

IV. CONCLUSION

We examined three features that describe the reaching movement of a human upper limb on a horizontal plane: the muscle synergy, endpoint stiffness, and EP trajectory. We proposed the novel muscle synergy extraction method, compared the endpoint stiffness and EP trajectory estimated from muscle synergy analysis with those from the perturbation method, and clarified that: (1) The movements of a human upper limb are composed of three muscle synergies. (2) Each muscle synergy is described by the balance of the coactivation of antagonistic muscle pair groups. (3) The first and second muscle synergies are invariable and help regulate the endpoint EP in the radial and angular directions, respectively. (4) The third muscle synergy is also invariable and helps regulate the endpoint stiffness. Beyond the scope of this paper, this extraction method can be adapted to EMG signals of a lower limb during walking movements; the extracted synergies are very similar to those of an upper limb. Therefore, this extraction method may help elucidate the interaction of the EP trajectory, endpoint stiffness, and muscle synergies.

REFERENCES

- [1] M. L. Latash, *Synergy*, Oxford University Press, 2008.
- [2] N. Bernstein, *The co-ordination and regulation of movements*, Oxford, Pergamon Press, 1967.
- [3] D. Shin, J. Kim and Y. Koike, "A myokinetic arm model for estimating joint torque and stiffness," *J. Neurophysiol.*, vol. 101, no. 1, pp. 387–401, 2009.
- [4] A. d' Avella, P. Saltiel, and E. Bizzi, "Combinations of muscle synergies in the construction of a natural motor behavior," *Nat. Neurosci.*, vol. 6, no. 3, pp. 300–308, 2003.
- [5] A. G. Feldman, S. V. Adamovich, D. J. Ostry, and J. R. Flanagan, "The origin of electromyograms - explanations based on the equilibrium point hypothesis," *Multiple Muscle Systems*, pp. 195–213, 1990.
- [6] P. K. Artemiadis, and K. J. Kyriakopoulos, "EMG-based control of a robot arm using low-dimensional embeddings," *IEEE Trans. Robo.*, vol.26, no. 2, pp. 393–398, 2010.
- [7] M. Santello, M. Flanders, and J. F. Soechting, "Postural hand synergies for tool use," *J. Neurosci.*, vol. 18, no. 23, pp. 10105–10115, 1998.
- [8] H. Gomi, and M. Kawato, "Human arm stiffness and equilibrium-point trajectory during multi-joint movement," *Biol. Cybern.*, vol. 76, no. 3, pp. 163–171, 1997.
- [9] H. T. T. Pham, Y. Ariga, K. Tominaga, T. Oku, K. Nakayama, M. Uemura, H. Hirai, and F. Miyazaki, "Extraction and implementation of muscle synergies in neuro-mechanical control of upper limb movement," *Adv. Robo.*, vol. 28, no. 11, pp. 745–757, 2014.
- [10] T. Iimura, K. Inoue, H. T. T. Pham, H. Hirai, and F. Miyazaki, "Decomposition of limb movement based on muscular coordination during human running," *J. Adv. Comp. Intel. Intel. Info.*, vol. 15, no. 8, pp. 980–987, 2011.
- [11] Y. Ariga, D. Maeda, H. T. T. Pham, M. Uemura, H. Hirai, and F. Miyazaki, "Novel Equilibrium-Point Control of Agonist-Antagonist System with Pneumatic Artificial Muscles: II. Application to EMG-based human-machine interface for an elbow-joint system," *Proc. IEEE/R SJ Int. Conf. Intelligent Robots and Systems (IROS2012)*, pp. 4380–4385, 2012.
- [12] K. Koba, K. Murakami, T. Oku, K. Uno, P. Pathiwattipat, Y. Yamashita, M. Uemura, H. Hirai, and F. Miyazaki, "Tacit representation of muscle activities during coordination training: Muscle synergy analysis to visualize motor enhancement in virtual trajectory of multi-joint arm movement," *Proc. 5th IEEE/RAS-EMBS Int. Conf. Biomed. Robot. Biomechatron. (BioRob2014)*, 2014. (accepted)